J|A|C|S
ARTICLES
Published on Web 12/03/2003

On the Nature of the Multivalency Effect: A Thermodynamic Model

Pavel I. Kitov* and David R. Bundle

Contribution from the Chemistry Department, University of Alberta, Edmonton, Canada T6G 2G2

Received August 29, 2003; E-mail: pkitov@ualberta.ca

Abstract: A quantitative model is proposed for the analysis of the thermodynamic parameters of multivalent interactions in dilute solutions or with immobilized multimeric receptor. The model takes into account all bound species and describes multivalent binding via two microscopic binding energies corresponding to inter- and intramolecular interactions (ΔG°_{inter} and ΔG°_{intra}), the relative contributions of which depend on the distribution of complexes with different numbers of occupied binding sites. The third component of the overall free energy, which we call the "avidity entropy" term, is a function of the degeneracy of bound states, Ω_i, which is calculated on the basis of the topology of interaction and the distribution of all bound species. This term grows rapidly with the number of receptor sites and ligand multivalency, it always favors binding, and explains why multivalency can overcome the loss of conformational entropy when ligands displayed at the ends of long tethers are bound. The microscopic parameters ΔG°_{inter} and ΔG°_{intra} may be determined from the observed binding energies for a set of oligovalent ligands by nonlinear fitting with the theoretical model. Here binding data obtained from two series of oligovalent carbohydrate inhibitors for Shiga-like toxins were used to verify the theory. The decavalent and octavalent inhibitors exhibit subnanomolar activity and are the most active soluble inhibitors yet seen that block Shiga-like toxin binding to its native receptor. The theory developed here in conjunction with our protocol for the optimization of tether length provides a predictive approach to design and maximize the avidity of multivalent ligands.

Introduction

Nature frequently uses multivalency to achieve tight binding in situations where univalent protein−ligand binding is weak.[1] Recognition of carbohydrate ligands by bacterial and mammalian lectins are examples of this phenomena, and specific inhibition of recognition events of this type have been proposed as therapeutic modalities for neutralization of bacterial toxins[2] and the prevention of viral[3] and bacterial infection.[4] The creation of tight binding multivalent inhibitors is for the most part a highly empirical endeavor. Tailored multivalency where the spacing of a limited number of tethered branches is matched to that between adjacent sugar binding sites of a protein can lead to rarely observed avidity gains,[5] but the thermodynamic basis for such gains has thus far eluded description. We develop here a quantitative treatment that accounts for these avidity gains.

The bacterial AB_5 toxins represent a conveniently uncomplicated system, in which to investigate multivalency. The ligand binding sites are displayed across one surface of disklike, radially symmetric B_5 subunits, and in principle, a multivalent ligand with related symmetry has the potential to engage all the highest affinity binding sites. Our treatment of this system utilizes the additivity of free energies,[1c] an approach suggested by Jencks[6] to account for the increase in binding affinity upon oligovalent interactions.

$$\Delta G^\circ_{multi} = i\Delta G^\circ_{mono} + \Delta G^\circ_{interaction} \quad (1)$$

where, ΔG°_{mono} is the binding energy of the corresponding monovalent interaction between a binding site of the receptor and a branch of the ligand, i represents the valency of the complex, and $\Delta G^\circ_{interaction}$ is a balance between the favorable and unfavorable effects of tethering.

However, for our purposes, we must adapt the above expression for the situation where the ligands and receptors consist of uniform binding elements. This requires a statistical factor to register the numerous ways equivalent bound forms may be achieved. This creates a statistical component that grows nonlinearly as the degree of multivalency increases. To arrive at a general approach, we introduce a further modification to take into account the free energy contributions of all partially bound species.

When these factors are considered we can demonstrate in detail the relationship between the experimentally accessible,

(1) (a) Lee, R. T.; Lee, Y. C. *Glycoconjugate J.* **2000**, *17*, 543−551. (b) Mammen, M.; Choi, S. K.; Whitesides, G. M. *Angew. Chem., Int. Ed.* **1998**, *37*, 2755−2794. (c) Lundquist, J. J.; Toone, E. J. *Chem. Rev.* **2002**, *102*, 555−578.
(2) St. Hillaire, P. M.; Boyd, M. K.; Toone, E. J. *Biochemistry* **1994**, *33*, 14452−14463.
(3) (a) Glick, G.; Knowles, J. R. *J. Am. Chem. Soc.* **1991**, *113*, 4701−4703. (b) Glick, G. D.; Toogood, P. L.; Wiley, D. C.; Skehel, J. J.; Knowles, J. R. *J. Biol. Chem.* **1991**, *266*, 23660−23669. (c). Sigal, G. B.; Mammen, M.; Dahmann, G.; Whitesides, G. M. *J. Am. Chem. Soc.* **1996**, *118*, 3789−3800. (d) von Itzstein, M.; Wu, W.-Y.; Kok, G. B.; Pegg, M. S.; Dyason, J. C.; Jin, B.; Phan, T. V.; Smythe, M. L.; White, H. F.; Oliver, S. W.; Colman P. M.; Varghese, J. N.; Ryan, D. M.; Woods, J. M.; Bethell, R. C.; Hotham, V. J.; Cameron, J. M.; Penn, C. R. *Nature* **1993**, *363*, 418−423.
(4) Sharon, N.; Ofek, I. *Glycoconjugate J.* **2000**, *17*, 659−664.
(5) Kitov, P. I.; Sadowska, J. M.; Mulvey, G.; Armstrong, G. D.; Ling, H.; Pannu, N. S.; Read, R. J.; Bundle, D. R. *Nature* **2000**, *403*, 669−672.

apparent association constant and the microscopic thermodynamic parameters, with an emphasis on the crucial role of the statistical nature of the interaction, a term, which we will call "avidity entropy".

We recently reported the subnanomolar activity of a decavalent carbohydrate-based ligand **9** (referred to as STARFISH) that was tailored to fit 10 of 15 binding sites presented across the relatively flat surface of the homopentameric B_5 portion of the Shiga-like toxin secreted by pathogenic *Escherichia coli* O157:H7.[5] This design principle was recently emulated by Hol and co-workers to create a similar decavalent inhibitor of cholera toxin.[7] We have also shown that appropriately tethered bivalent ligands form complexes, in which both site 2 and the less active site 1 of each B_5 subunit of SLT-1 are simultaneously occupied.[8] Here we describe the activities of oligovalent inhibitors tailored to bind to these sites in different B subunits. The common feature of these ligands is a central core with pseudo *n*-fold symmetry, in this case a glucopyranoside. Attached to the tips of tethers that radiate from the glucopyranoside are mono- and dimeric P^k-trisaccharides. The decavalent and pentavalent molecules represent the maximum *valency* of two series of ligands wherein the *multivalency* is limited to three, four, and five tethers each capped by either P^k-trisaccharides or P^k-trisaccharide dimers. An analogous 8-valent ligand based on the PAMAM dendrimer is also included in the set of univalently branched ligands. The activities of these oligovalent ligands in a solid-phase assay are used to evaluate the thermodynamic model developed to explain multivalency effects.

A valid thermodynamic model combined with computational modeling will permit the prediction of binding activities of diverse multivalent ligand designs, and remove a significant degree of the serendipity that accompanies attempts to synthesize high-avidity multivalent ligands.

Development of a Thermodynamic Model

The general approach adopted here considers the contribution of all bound species and their distribution, while concentration refers to that of the whole multivalent molecule and not an average per binding site concentration. There is a tendency in the literature to express concentrations of multivalent components and even thermodynamic parameters as an average per binding site and/or per branch of ligand. Although convenient for measuring drug efficacy such "valency-corrected" data obscure the statistical aspect of the binding mechanism. The statistical components of binding energy grow nonlinearly with increase in the degree of multivalency and, except in particular cases, their effect cannot be adjusted by choosing a different concentration scale. We show here that valid thermodynamic analysis of binding data can only be achieved by expressing concentrations on a *whole molecule* basis.

We consider an interaction between an oligomeric protein receptor and a multivalent ligand under the following limiting conditions: (1) Only one multivalent ligand can bind to the oligomeric receptor at a time; steric hindrance precludes any further interaction even with unoccupied binding sites. Thus, no aggregates are considered. (2) All *n* binding sites of the multimeric protein receptor R and *m* branches of the multivalent ligand L act independently and have identical binding properties.

Let us consider formation of a *microscopic* complex rl(*i*) between the multivalent receptor R and ligand L, which has a unique arrangement between *i* binding sites of the receptor occupied by *i* branches of the ligand. According to Jencks' principle of additivity of binding energies,[6] the free energy of formation of the complex rl(*i*) is

$$\Delta g_i^\circ = i\Delta G_{\text{mono}}^\circ + \Delta G_{\text{interaction}}^\circ \qquad (2)$$

The $\Delta G_{\text{interaction}}^\circ$ is introduced by Jencks to correct for imperfections in additivity arising from the difference between free energies of the initial intermolecular and subsequent intramolecular binding events. Hence, $\Delta G_{\text{interaction}}^\circ$ is the result of the intramolecular nature of the subsequent interactions. To facilitate the thermodynamic analysis we rearrange the terms in eq 2 according to the origin of interactions, so that the contribution of the initial binding event is designated as intermolecular free energy $\Delta G_{\text{inter}}^\circ = \Delta G_{\text{mono}}^\circ$ and is separated from the free energies of all subsequent interactions $(i-1)\Delta G_{\text{intra}}^\circ = (i-1)\,\Delta G_{\text{mono}}^\circ + \Delta G_{\text{interaction}}^\circ$. Thus, the free energy of the complex rl(*i*) will be represented as a result of a sequential rather than concerted process:

$$\Delta g_i^\circ = i\Delta G_{\text{inter}}^\circ + (i-1)\Delta G_{\text{intra}}^\circ \qquad (3)$$

Since all binding units of the ligand and receptor have identical binding properties, all *microscopic* complexes rl(*i*) with *i* binding sites engaged have identical free energies and can be collectively represented by a *macroscopic* complex RL(*i*). The degeneracy coefficient Ω_i is introduced to reflect the fact that a complex designated as RL(*i*) is not an individual molecule but an ensemble of Ω_i microscopically distinguishable complexes rl(*i*). The free energy of complex RL(*i*) formation is found as

$$\Delta G_i^\circ = \Delta G_{\text{inter}}^\circ + (i-1)\Delta G_{\text{intra}}^\circ - RT\ln\Omega_i \qquad (4)$$

The isothermal equilibrium distribution of species according to their respective energy levels is governed by a Boltzmann-like distribution law. Since the macroscopic complex RL(*i*) with *i* number of engaged binding sites is represented by a degenerate free energy level, ΔG_i°, the probability of an individual *i*th bound level is found as a partial average over all bound states of the receptor:

$$w_i = \frac{e^{-\Delta G_i^\circ/RT}}{\sum_{i=1}^{i_{\max}} e^{-\Delta G_i^\circ/RT}} \qquad (5)$$

The contribution of each bound species RL(*i*) to the overall free energy of the complex RL is proportional to the corresponding weight coefficient w_i. However, to obtain the expression for overall free energy we must first define the overall binding constant.

Definition for Avidity Binding Constant. There is a controversy in describing the activity of multivalent ligands.[1,9,10]

(6) Jencks, W. P. *Proc. Natl. Acad. Sci. U.S.A.* **1981**, *78*, 4046−50.
(7) Zhang, Z.; Merritt, E. A.; Ahn, M.; Roach, C.; Hou, Z.; Verlinde, C. L. M. J.; Hol, W. G. J.; Fan, E. *J. Am. Chem. Soc.* **2002**, *124*, 12991−12998.
(8) Kitov, P. I.; Shimizu, H.; Homans, S. W.; Bundle, D. R. *J. Am. Chem. Soc.* **2003**, *125*, 3284−3294.
(9) (a) Helg, A.; Mueller, M. S.; Joss, A.; Poltl-Frank, F.; Stuart, F.; Robinson, J. A.; Pluschke, G. *J. Immunol. Methods* **2003**, *276* (1−2), 19−31. (b) Mattes, M. J. *J. Immunol. Methods* **1997**, *202*, 97−101.

Depending on how the signal is generated and what bound species contribute to it, the same ligand may show different activity to the same receptor when measured by different analytical techniques.[9a] The arbitrary nature of activity measurements is underscored by such adjectives as "effective", "functional", "pseudo", "observed", and "apparent" appended to the binding constant. However, an unambiguous thermodynamic definition for the binding constant can be given as the ratio between products and reactants, when the concentration of products is defined as the sum of all possible complexes.

$$\mathrm{R} + \mathrm{L} \overset{K_{\mathrm{avidity}}}{\rightleftharpoons} \mathrm{RL}(1) + \mathrm{RL}(2) + \ldots + [\mathrm{RL}(i)] + \ldots$$

$$K_{\mathrm{avidity}} = \frac{\sum[\mathrm{RL}(i)]}{[\mathrm{R}][\mathrm{L}]} = \frac{[\mathrm{R}_{\mathrm{bound}}]}{[\mathrm{R}][\mathrm{L}]} = \frac{[\mathrm{R}]_{\mathrm{o}} - [\mathrm{R}]}{[\mathrm{R}][\mathrm{L}]} \qquad (6)$$

where [R], [R_{bound}], and $[R]_o$ are unbound, bound, and total concentrations of the receptor, respectively.

Although the term "avidity" is usually considered a nonquantitative description of multivalent binding, we suggest the term "avidity binding constant" for this exactly defined thermodynamic parameter (for multivalent systems subject to limiting condition 1; in case of aggregation, $K_{avidity}$ is an extrapolation to infinite dilution of the receptor). This definition of overall binding constant $K_{avidity}$ is consistent with the term "functional affinity" originally introduced by Karush[10] and differs from the definition given by Whitesides[1b] as $K_{avidity} = (K_{average})^N$.

All bound species of the receptor are treated collectively, and $K_{avidity}$ represents their cumulative effect. When the binding isotherm is presented in [R] − [L] coordinates, it assumes the familiar shape of the Langmuir isotherm. In addition to being general and accurate, this is also a very convenient operational definition. Indeed, at the midpoint of the binding isotherm, $[R] = 0.5[R_o] = \Sigma[RL(i)]$ and $[L] = IC_{50}$. Therefore, under conditions of excess ligand, $K_{avidity}$ is the reciprocal of IC_{50} obtained by monitoring the concentration of the *unbound* form of the multivalent receptor [R] or combined concentration of all bound species of the receptor $\Sigma[RL(i)]$. We explain how the solid-phase assay achieves this objective in the Discussion.

$$K_{\mathrm{avidity}} = \frac{1}{\mathrm{IC}_{50}} \qquad (7)$$

Thus, the avidity binding constant is a convenient intuitive parameter, which can be used for evaluating the activity of multivalent ligands.

Equation 6 defines $K_{avidity}$ as a sum of constants of complex formation for individual bound species.

$$K_{\mathrm{avidity}} = \sum_{i=1}^{i_{\max}} K_i \qquad (8)$$

Although each binding constant K_i has an unambiguous thermodynamic meaning and can be expressed in terms of free energy, the conversion of $K_{avidity}$ to avidity free energy assumes a mathematically awkward form, the logarithm of a sum:

$$\Delta G^{\circ}_{\mathrm{avidity}} = -RT \ln \sum_{i=1}^{i_{\max}} K_i = -RT \ln \sum_{i=1}^{i_{\max}} \mathrm{e}^{-\Delta G^{\circ}_i/RT} \qquad (9)$$

Nevertheless, using the knowledge of the distribution of bound species at equilibrium (eq 5) it is possible to expand the series in eq 9 and separate three terms corresponding to different forms of free energy: inter- and intramolecular free energies and a degeneracy term (see Supporting Information).

$$\Delta G^{\circ}_{\mathrm{avidity}} = \Delta G^{\circ}_{\mathrm{inter}} + \Delta G^{\circ}_{\mathrm{intra}} \sum_{i=1}^{i_{\max}} \mathrm{w}_i (i-1) + RT \sum_{i=1}^{i_{\max}} \mathrm{w}_i \ln (\mathrm{w}_i/\Omega_i) \qquad (10)$$

This expression is important for a thermodynamic analysis of multivalent interactions. All enthalpic effects of the multivalent interaction are contributed by the first two terms of eq 10: the enthalpy portions of the inter- and intramolecular binding energies. The first term ΔG°_{inter} is similar to the free energy of the intrinsic monovalent interaction ΔG°_{mono}, whereas the second and the third terms in eq 10 constitute two facets of the multivalency effect: additional specific interactions and the effect of a statistical factor.

The magnitude of the second term in eq 10 depends on the maximal number of additional intramolecular interactions ($i_{max} - 1$) so that the maximal value of the second term, $(i_{max} - 1)\Delta G^{\circ}_{intra}$, is never achieved but asymptotically approached as the number of branches in the multivalent ligand increases (Figure 1).

The form of the statistical term $-R\Sigma w_i \ln(w_i/\Omega_i)$ in eq 10 agrees with the generalized Bolttzmann−Gibbs definition of entropy[12] and is expressed in entropy units. Since this term represents the probability of the interaction rather than its strength, we will refer to it as "avidity entropy", $\Delta S^{\circ}_{avidity}$. This type of entropy is unique to multivalent interactions; it is a measure of disorder in the distribution of microscopically distinct complexes. Avidity entropy is always positive and favors association of multivalent ligand and multivalent receptor. Its magnitude can become substantial as the number of binding sites per protein receptor and the number of branches of the ligand increase.

If we expand the expression for avidity entropy into two terms, the generality of our model can be appreciated:

$$\Delta S^{\circ}_{\mathrm{avidity}} = -R \sum_{i=1}^{i_{\max}} \mathrm{w}_i \ln \mathrm{w}_i + R \sum_{i=1}^{i_{\max}} \ln \Omega_i \qquad (11)$$

For a better understanding of the nature of the avidity entropy consider an extreme situation. Suppose $\Delta G^{\circ}_{intra} = 0$ kcal/mol, i.e., microscopic complexes have equal free energies and equal probabilities. The degeneracy of the states is maximal $\Omega = \Sigma\Omega_i$. Then the probability of this level equals unity ($w = 1$); therefore,

(10) Karush, F. The affinity of antibody: range, variability and the role of multivalence. In *Comprehensive Immunology, Immunoglobulins*; Plenum Press: New York, 1978; pp 85−116.

(11) (a) Dimick, S. M.; Powell, S. C.; McMahon, S. A.; Moothoo, D. N.; Naismith, J. H.; Toone, E. J. *J. Am. Chem. Soc.* **1999**, *121*, 10286−10296. (b) Corbell, J. B.; Lundquist, J. J.; Toone, E. J., *Tetrahedron*: *Asymmetry* **2000**, *11*, 95−111. (c) Lundquist, J. J.; Debenham, S. D.; Toone, E. J. *J. Org. Chem.* **2000**, *65*, 8245−8250. (d) Dam, T. K.; Roy, R.; Das, S. K.; Oscarson, S.; Brewer, C. F., *J. Biol. Chem.* **2000**, *275*, 14223−14230. (e) Dam, T. K.; Brewer, C. F.; Das, S. K.; Roy, R. *Glycobiology* **2001**, *11*, 189.

(12) Chakrabarti, C. G.; De, K. *Internat. J. Math., Math. Sci*. **2000**, *23*(4), 243−251.

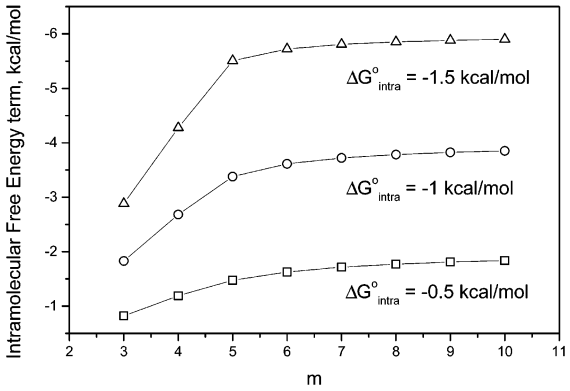

Figure 1. Dependence of the intramolecular energy (second term in eq 10) on the number of branches in a multivalent ligand (m) and intramolecular free energy ($\Delta G^{\circ}_{\text{intra}}$) with respect to the pentameric receptor (number of binding sites $n = 5$). The magnitude of activity amplification due to intramolecular interactions asymptotically approaches $(n - 1)\Delta G^{\circ}_{\text{intra}}$.

the first term in the eq 11 cancels out, and we have the avidity entropy equal to the Boltzmann term only:

$$\Delta S^{\circ}_{\text{avidity}} = R \ln \Omega \tag{12}$$

On the other hand, we may think of this system as if it consisted of ensemble of individual bound states with equal probabilities w_i. Then the summation must be conducted over $i_{\max} = \Omega$ equal states. The degeneracy of each individual state in the ensemble is unity ($\Omega_i = 1$); hence, the second term in eq 11 cancels out, and we have the Shannon expression for avidity entropy:

$$\Delta S^{\circ}_{\text{avidity}} = -R\sum_{i=1}^{\Omega} w_i \ln w_i \tag{13}$$

Both expressions give the same numerical result, but the first one is obviously computationally simpler. Thus, for our model, any assumption about the degeneracy of binding states is not absolutely necessary but greatly simplifies the calculation of avidity entropy. Conversely, deviations in free energies of bound states (violation of limiting condition 2) do not abolish the avidity entropy, although they may diminish its magnitude and complicate calculation.

The magnitude of the degeneracy factor Ω_i depends on the topology of multivalent interaction. To illustrate the point, four elementary topologically distinct modes of binding are shown in Figure 2.

In case of *indifferent topology*, only one branch of a cluster can specifically interact with the binding site. Regardless of the particular arrangement of the active fragments in the ligand, the tethers are too short to allow other branches in the cluster to reach the nearest binding site. Since no intramolecular interactions are possible, there is only one bound level, and activity enhancement is minimal. The degeneracy for this level is

$$\Omega(\text{indifferent}) = nm \tag{14}$$

An example of *linear topology* is the interaction between ligand and receptor, each of which consists of uniform complementary nucleotide sequence (for instance a small repeating sequences). Due to the uniformity of binding units

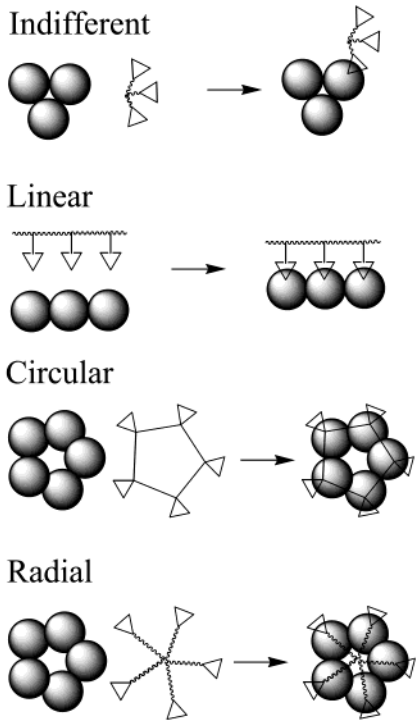

Figure 2. Topologies of multivalent interactions.

the number of complexes with the same number of nucleotides engaged greatly increases at the expense of linearly shifted complexes. When loops are not considered, the degeneracy of the *i*th bound level is

$$\Omega_i(\text{linear}) = (n - i + 1)(m - i + 1) \tag{15}$$

An example of *circular topology* is an artificial binding system designed by Whitesides and co-workers.[13] Rigid linkers hold several copies of vancomycin in one plane at the same distance from the central core; its binding partner with a D-Ala-D-Ala sequence specifically recognized by vancomycin is constructed in the same way to facilitate the interaction. After initial interaction between a branch of the ligand with a binding site takes place, each next branch has "designated" binding sites with which it can only interact. The degeneracy in this case is

$$\Omega_i(\text{circular}) = nm \tag{16}$$

except for the complex when $n = m = i_{\max}$, which has degeneracy equal to n.

There are only a few pure examples of *radial topology*. The interactions of tailored pentavalent ligands with pentameric bacterial toxins[5,7] are some of them. The ligand is a symmetrical or pseudosymmetrical molecule with several copies of active fragment tethered to a multivalent core. The tethers must be sufficiently long and flexible to permit interaction of each branch with each binding site of a multivalent receptor. Since there are no topological restrictions, each binding site is equally accessible to each receptor subunit. Therefore, the number of energetically equivalent bound states and the degeneracy are maximal.

(13) Rao, J.; Lahiri, J.; Isaacs, L.; Weis, R. M.; Whitesides, G. M. *Science* **1998**, *280*, 708−711.

$$\Omega_i(\text{radical}) = \frac{n!m!}{(n-i)!(m-i)!i!} \qquad (17)$$

Combinations of these modes are more common than the idealized forms. In particular, the indifferent presentation can be found, to some degree, in the vast majority of scaffold designs of multivalent inhibitors. Although these nonreacting branches do not contribute to the enthalpy of binding they do increase the probability of interaction and, therefore, contribute favorable entropy. The branches that are not engaged in the principle interaction are responsible for secondary effects such as aggregation and precipitation.[14]

The contribution of the avidity entropy to the avidity free energy in the case of radial topology is shown in Figure 3. The influence of $\Delta G^\circ_{\text{intra}}$ on the magnitude of the $\Delta S^\circ_{\text{avidity}}$ term is very limited, and even at $\Delta G^\circ_{\text{intra}} = 0$ the model predicts a substantial increase in binding energy compared to a univalent interaction. This suggests that, in the first approximation, the value of $\Delta S^\circ_{\text{avidity}}$ can be calculated as a Boltzmann entropy, $R \ln \Sigma\Omega_i$ (eq 12).

Several practical inferences can be drawn from Figure 3. For example, when a protein such as IgG with only two binding sites interacts with a multivalent ligand, avidity gains must derive from the term $\Delta G^\circ_{\text{intra}}$, since gains from avidity entropy are limited. In sharp contrast, a receptor with 10 sites (for example IgM) can make substantial avidity gains from interactions with a multivalent ligand; even when individual interactions contribute very little, the third term (avidity entropy) becomes substantial. It is often reasoned that loss of torsional entropy by tethered species containing multiple single bonds should be expected to render avidity gains of very small magnitude;[15] however, even if the torsional entropy term reduces $\Delta G^\circ_{\text{intra}}$ to zero, it will not significantly affect the $\Delta S^\circ_{\text{avidity}}$ term, which can still drive the association (Figure 3).

Finding Microscopic Binding Parameters from Binding Data. Compared to a monovalent interaction, the thermodynamic analysis of a multivalent system cannot be based on binding measurements for a single ligand−receptor pair, because an infinite number of combinations for $\Delta G^\circ_{\text{inter}}$ and $\Delta G^\circ_{\text{intra}}$ would satisfy eq 10. However, these parameters may be deduced from a *set* of IC_{50} values for analogous multivalent ligands with varying numbers of branches.

Consider an interaction between a multivalent receptor and several (at least two) analogous multivalent ligands that only differ in the number of independent branches. After the avidities of these ligands are measured in a binding experiment we may construct a fitting function 18 from the difference between *experimental* avidity free energy $\Delta \check{G}^\circ_{\text{avidity}}$ and *calculated* avidity free energy $\Delta G^\circ_{\text{avidity}}$. The latter is obtained by eq 9 or 10 on the basis of variable values of $\Delta G^\circ_{\text{inter}}$ and $\Delta G^\circ_{\text{intra}}$:

$$\chi^2 = \frac{\sum_{i=1}^{k} [\Delta \check{G}^\circ_{\text{avidity}}(i) - \Delta G^\circ_{\text{avidity}}(i)]^2}{k} \qquad (18)$$

The goodness-of-fit χ^2 is a function of two parameters: $\Delta G^\circ_{\text{inter}}$ and $\Delta G^\circ_{\text{intra}}$. Simultaneous variation of these parameters results in a curved surface with a global minimum, which can be found at the bottom of a narrow groove by a grid search (Figure 4).

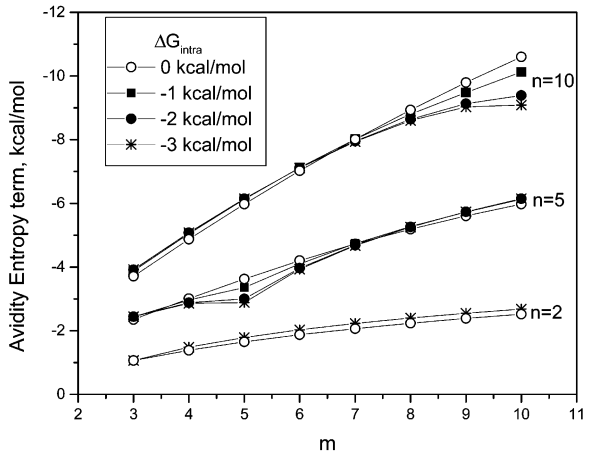

Figure 3. Dependence of the avidity entropy term in eq 10 on the number of branches in the multivalent ligand (m) and intramolecular free energy ($\Delta G^\circ_{\text{intra}}$) with respect to the *n*-meric receptors (number of binding sites $n = 2$, 5, or 10). The graph demonstrates that avidity increase due to $\Delta S^\circ_{\text{avidity}}$ term is relatively independent of the magnitude of intramolecular interaction and, at all nonpositive $\Delta G^\circ_{\text{intra}}$, provides a substantial contribution to overall binding energy. Calculations are based on radial binding topology (eq 17).

Design of Inhibitors. We consider here the interaction of the Shiga-like toxin Type 1 (SLT-1) with a series of clustered multivalent oligosaccharide ligands. A pseudoradially symmetric, cluster-shaped, multivalent ligand consisting of long flexible branches, seems to provide an adequate model for the multivalent system described in the previous section.

The native ligand for Shiga-like toxins (SLT) is the carbohydrate portion of the Gb_3 glycolipid, the oligosaccharide portion of which is referred to as P^k-trisaccharide, α-D-Gal*p*-(1→4)-*β*-D-Gal*p*-(1→4)-*β*-D-Glc*p*. According to the solved crystal structure of the protein−trisaccharide complex, the doughnut-shaped homopentameric binding subunit SLT-1(B_5) has 15 P^k-binding sites of three different types.[16] All available data suggest that, of three distinct binding sites for the P^k-trisaccharide on the surface of SLT-1, site 2 dominates in solution.[2,17,18] Its association constant $K_a^{\text{site 2}} \approx 1-0.5 \times 10^3$ was measured by isothermal titration microcalorimetry.[2] The binding constant for site 1 ($K_a^{\text{site 1}}$), which appears to be the next in activity, is estimated to be only 10−15% that of $K_a^{\text{site 2}}$.[17] Site 3, which is positioned close to the center of the toxin, does not significantly contribute to affinity but is believed to guide the interaction with multivalent ligands by rapid and transient binding, thus preventing intertoxins cross-linking in solution.[18] Due to the substantial difference in activities between site 1 and site 2 the trisaccharides are expected to target the most avid binding site 2. Hence, in the first approximation, the affinity of Shiga-like toxin to its ligand is determined by the five equivalent, most avid binding sites (see Scheme 1).

(14) Burke, S. D.; Zhao, Q.; Schuster, M. C.; Kiessling, L. L. *J. Am. Chem. Soc.* **2000**, *122*, 4518−4519.
(15) (a) Mammen, M.; Shakhnovich, E. I.; Whitesides, G. M., *J. Org. Chem.* **1998**, *63*, 3168−3175. (b) Burkhalter, N. F.; Dimick, S. M.; Toone, E. J. In *Protein-Carbohydrate Interaction: Fundamental Considerations. Carbohydrates in Chemistry and Biology*; Ernst, G. W. H. B., Sinay, P., Eds.; Wiley-VCH: New York, 2000; pp 865−914.
(16) Ling, H.; Boodhoo, A.; Hazes, B.; Cummings, M. D.; Armstrong, G. D.; Brunton, J. L.; Read, R. J. *Biochemistry* **1998**, *37*, 1777−1788.
(17) (a) Richardson, J. M.; Evans, P. D.; Homans, S. W.; Donohue-Rolfe, A. *Nat. Struct. Biol.* **1997**, *4*, 190−193. (b) Kitova, E. N.; Kitov, P. I.; Bundle, D. R.; Klassen, J. S. *Glycobiology* **2001**, *11*, 605−611.
(18) Soltyk, A. M.; MacKenzie, C. R.; Wolski, V. M.; Hirama, T.; Kitov, P. I.; Bundle, D. R.; Brunton, J. L. *J. Biol. Chem.* **2002**, *277* (7), 5351−5359.

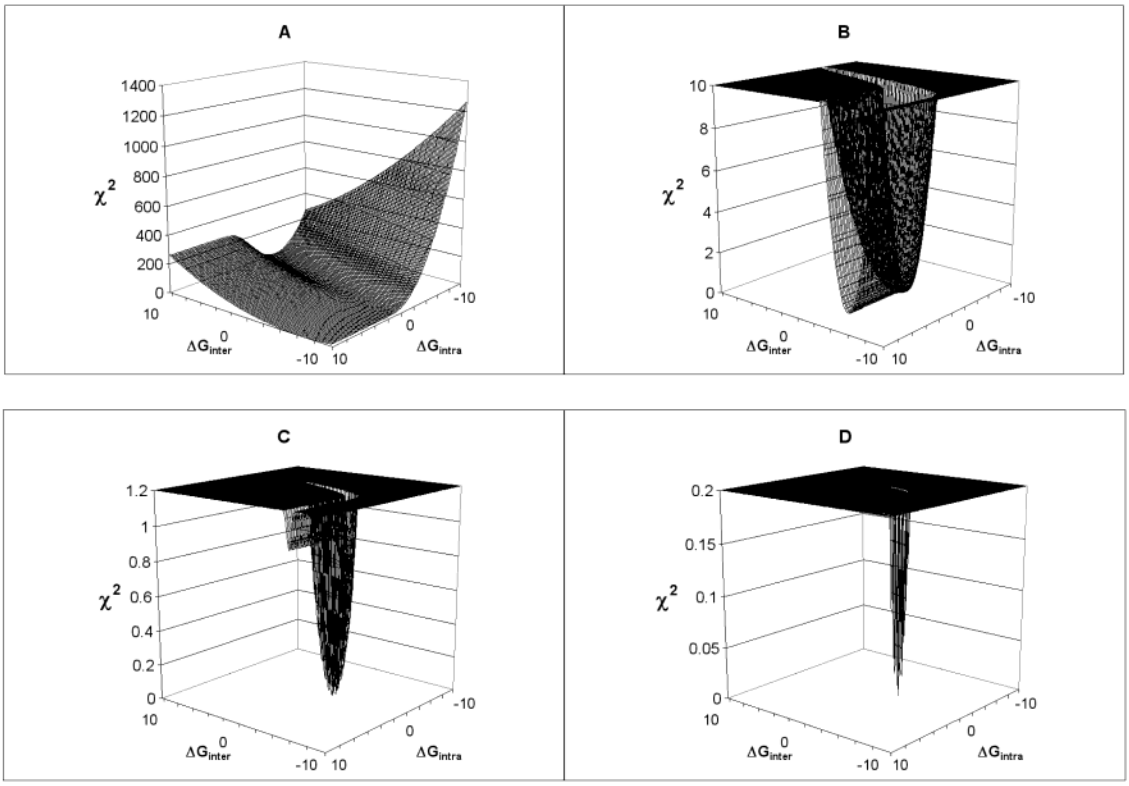

Figure 4. Three-dimensional plot of χ^2 (eq 18) as a function of two variable parameters $\Delta G^\circ_{\text{inter}}$ and $\Delta G^\circ_{\text{intra}}$. For generation of the "experimental" set of $\Delta G^\circ_{avidity}$ the following parameters were used: $\Delta G^\circ_{\text{inter}} = -2$ kcal/mol and $\Delta G^\circ_{\text{intra}} = -1$ kcal/mol, $n = 5$, $m = 3$, 4, and 5. Panel A is an overview of the χ^2 surface, Panels B−D show, on a progressively finer scale, the groove converging to the global minimum with $\Delta G^\circ_{\text{inter}} = -2$ kcal/mol and $\Delta G^\circ_{\text{intra}} = -1$ kcal/mol.

Scheme 1

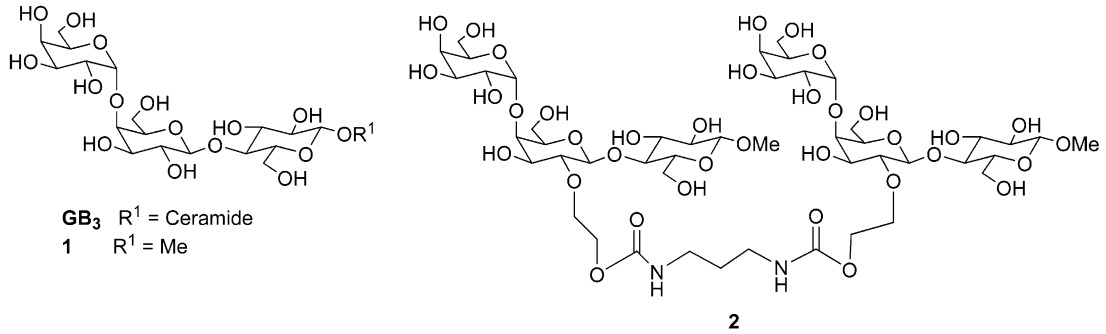

Owing to the pentagonal arrangement of carbohydrate binding pockets on the protein surface, the bound trisaccharides can be tethered to a common core molecule, which is positioned at the center of the pentagon. Accordingly, a series of tri-, tetra-, penta-, and octavalent clusters **3**, **4**, **5**, and **6** as well as structurally more complex tri-, tetra-, and pentavalent P^k-trisaccharide dimers **7**, **8**, and **9** were prepared (Scheme 2).

Long, flexible tethers link three, four, or five P^k-trisaccharide determinants to a relatively small core molecule, glucose in this case. The length of the linkers in the extended conformation is ~34 Å, a distance that is sufficient to cover the ~25 Å distance from the center of the B_5 homopentamer to the sugar attachment point. The exceptionally compact presentation of attachment points in a monosaccharide renders glucose an attractive core molecule in our study. The linker attached to the hydroxyl at C-6 is approximately 1 Å longer than the others but when compared to the total length of the linker this 3% difference was not expected to substantially influence binding properties of this branch.

Previously, we have demonstrated that alkyl substituents at *O*-2′ in P^k-trisaccharide do not significantly affect binding to Shiga-like toxin.[19] Hence, the hydroxyl group at the *C*-2′ position was chosen as an attachment point because of its proximity to the center, as compared with the anomeric position of the glucose residue of the P^k-trisaccharide, which if used for conjugation, would require the longest possible linker-arm. The octavalent analogue **6** is constructed on the basis of the PAMAM octaamino dendrimer.

The second series of ligands presents more complex assemblies of the branched 3-, 4-, or 5-meric ligands, in which P^k-trisaccharides are first assembled as dimers, which are then tethered to the core glucose molecule. This design was inspired

(19) Kitov, P. I.; Bundle, D. R. *J. Chem. Soc., Perkin Trans. 1* **2001**, 838−853.

Scheme 2

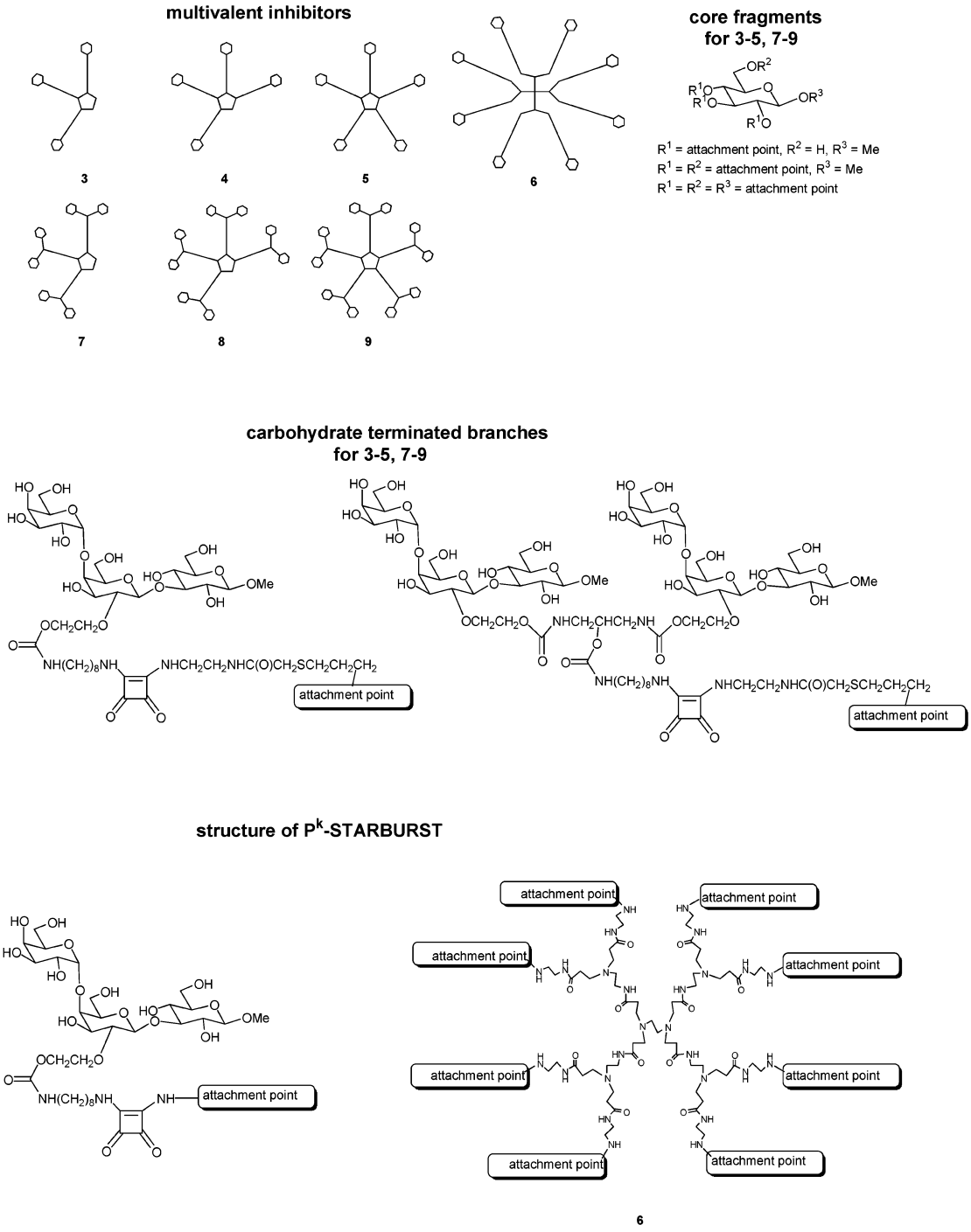

by an examination of the crystal structure of the P^k-trisaccharide complexed with SLT-1, which suggests opportunities for bridging two neighboring molecules of the trisaccharide bound to site 1 and site 2 respectively to create a specific ligand to a surrogate binding site {1;2}. As in the previous series of ligands we have chosen a nonglycosidic linkage between the two trisaccharides. The distance between *C*-2′ of two P^k-trisaccharides bound to site 1 and site 2 is only 10.8 Å, and the path is not obstructed by any protein features. The length of the spacer-arms that are necessary to connect the branches with the central fragment also constitutes a significant saving over linking via the glycosidic position, a feature that is invariably the default design of multivalent oligosaccharide inhibitors.

Hence, the design of the latter series combines two approaches for targeting the equivalent and nonequivalent binding sites found in the P^k−SLT-1 complex (Figure 5). The activity and mode of action for decavalent dendrimer **9** named STARFISH have been reported.[5] We briefly present here the previously unreported account of the synthesis of this potent SLT-1 inhibitor together with its attenuated analogues.

Synthesis of Inhibitors. Block assembly of the multivalent star-shaped inhibitors started with construction of the trisaccharide-bearing arms that were subsequently attached to a glucose-based core. Activated carbonate **10**[19] reacted with excess of 1,8-diaminooctane to give amine **11**, which was hydrogenated to afford the unprotected derivative **12**, which was in turn

Scheme 3

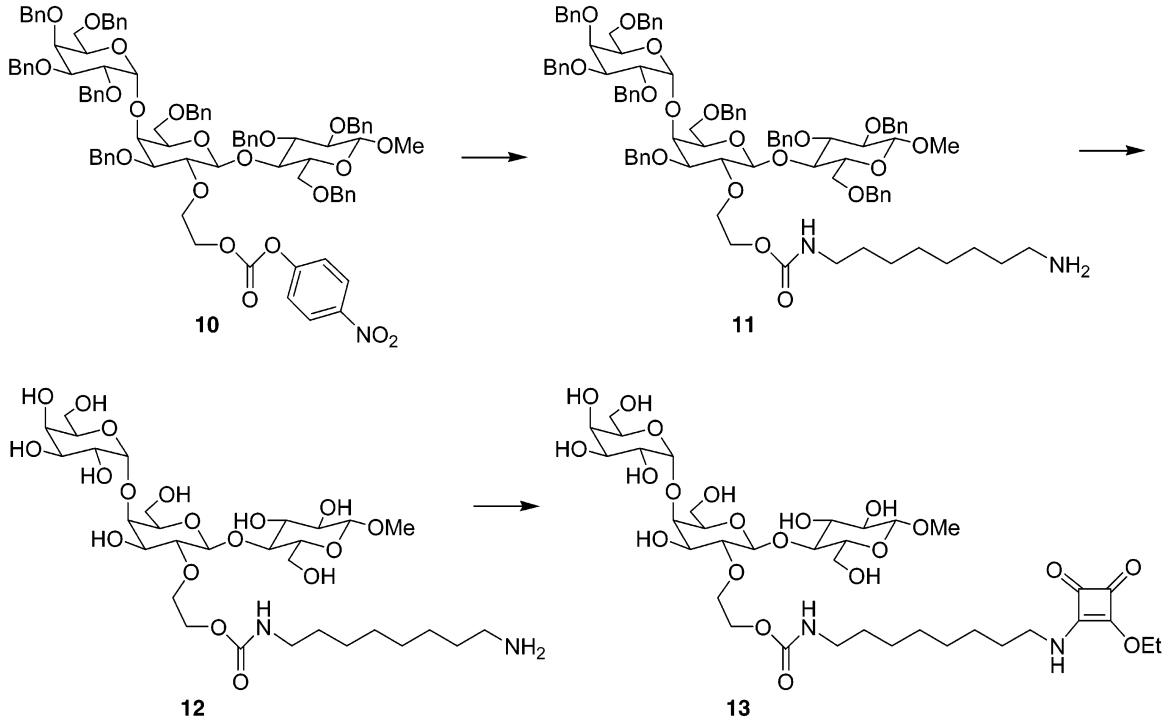

Scheme 4

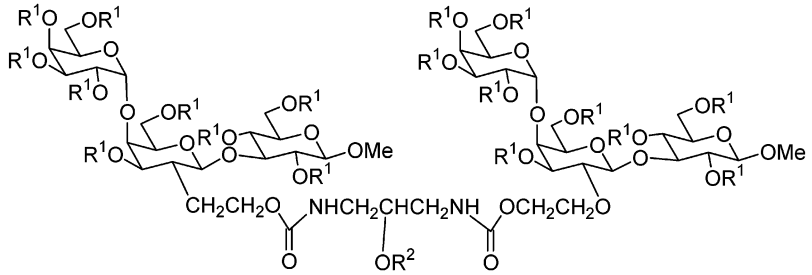

14 R^1= Bn, R^2 = H
15 R^1= Bn, R^2 = OC(O)O(p-C_6H_4)NO_2
16 R^1= Bn, R^2 = OC(O)NH$(CH_2)_8NH_2$
17 R^1= H, R^2 = OC(O)NH$(CH_2)_8NH_2$
18 R^1= H, R^2 = OC(O)NH$(CH_2)_8$NH

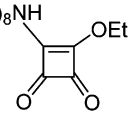

activated as a squaric acid semi-amide **13** (Scheme 3), a building block for P^k-trisaccharide-terminated dendrimers **3**−**6**.

Reaction of 1,3-diamino-2-hydroxypropane with excess of **10** in THF provided the bridged trisaccharide dimer **14**. Activation of the latter as its *p*-nitrophenyl carbonate **15** followed by the condensation with an excess of 1,8-diaminooctane yielded **16**. Hydrogenation of **16** gave the deprotected bridged P^k dimer with an amine-terminated linker **17**. The amino group of this spacer arm was activated as the squaric acid derivative **18** (Scheme 4), a building block for P^k-trisaccharide dimer terminated dendrimers **7**−**9**.

To make oligomeric scaffolds of varying multivalency, glucose was functionalized as follows. Selective tritylation of methyl β-D-glucopyranoside with TrCl in pyridine gave the 6-*O*-trityl derivative **19**,[20] the remaining hydroxyl groups of which were allylated and, finally, trityl group removal furnished the tri-*O*-allyl ether **20**. Tetra- and penta-*O*-allyl derivatives **23** and **26** were obtained by direct per-*O*-allylation of methyl β-D-glucopyranoside and D-glucose, respectively. Photoaddition of methyl mercaptoacetate to the double bonds of the tri-, tetra-, and penta-*O*-allyl derivatives of glucopyranose **20**, **23**, and **26** gave intermediates **21**, **24**, and **27**, respectively, with extended spacer-arms that were further elongated by condensation with ethylendiamine to provide the corresponding oligoamine-terminated scaffold molecules **22**, **25**, and **28** (Scheme 5). Finally, the series of P^k-trisaccharide clusters **7**−**9** were obtained by condensation of the corresponding oligoamines with either monomeric or dimeric squarate derivatives **13** and **18**. The resulting dendrimers were purified by reversed-phase HPLC using a water−methanol gradient as eluent. The structure and

(20) Rao, V. S.; Perlin, A. S. *Can. J. Chem.* **1983**, *61*, 2688−2694.

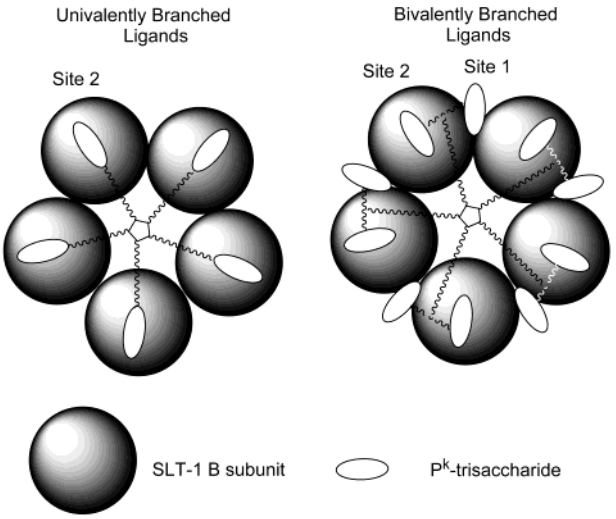

Figure 5. Putative modes of binding of monovalently and bivalently branched ligands with immobilized Shiga-like toxin.

purity were ascertained by NMR spectra and various mass-spectroscopy techniques, e.g. MALDI TOF and deconvolution of multiple charged ions in electrospray MS.

Activity Evaluation. Details of the solid-phase assay format have been previously reported.[5,19] In brief, the SLT-1 protein is immobilized on the wells of a microtiter plate. A glycoconjugate prepared from P^k-trisaccharide synthetically conjugated to BSA and biotinylated binds to the immobilized toxin, and the amount of bound biotin is measured by a biotin−streptavidin protocol, where immobilized biotin is quantified by a streptavidin−horseradish peroxidase conjugate. Incubation of this glycoconjugate reporter molecule in the presence of increasing amounts of inhibitor provides a dose response curve (Figure 6). This protocol shows a remarkably broad dynamic range and permits the assay of inhibitors with activities from mM to nM (see Table 1).

Thermodynamic analysis was conducted as described above. The activities of three univalently branched derivatives **3**, **4**, and **5** were used for χ^2 minimization according to eq 18, using either eq 9 or 10 to evaluate "calculated" $\Delta G^\circ_{\text{avidity}}$ and eqs 17 and 5 to obtain the degeneracy coefficient Ω_i for radial topology and distribution factors w_i. On the basis of obtained values of microscopic binding free energies (Table 2) the avidity energy (and the corresponding binding constant) for the fourth ligand in the series of univalently branched ligands **6** was predicted. As shown in Table 1 and Figure 7 the predicted activity shows excellent agreement with the experimental value.

As was mentioned before the rational behind the design of bivalently branched ligands of the second series **7**−**9** was that after one P^k-trisaccharide on the branch is bound to the highest affinity site 2 despite the fact that the second P^k-trisaccharide unit would be unable to reach any other site 2 on the protein surface (indifferent topology), it is able to engage the less active site 1, thereby enhancing its activity.[8] Accordingly, in calculation of the degeneracy coefficient by eq 17 each bivalent branch of **7**−**9** was treated as a single composite branch. Thus, compound **9**, for instance, was assigned $m = 5$.

Discussion

We have developed a thermodynamic model that describes multivalent binding at equilibrium in the absence of aggregation.

Scheme 5

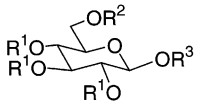

19 R^1 = H, R^2 = Tr, R^3 = Me
20 R^1 = All, R^2 = H, R^3 = Me
21 R^1 = $CH_2CH_2CH_2SCH_2C(O)OMe$, R^2 = H, R^3 = Me
22 R^1 = R^2 = $CH_2CH_2CH_2SCH_2C(O)NHCH_2CH_2NH_2$, R^2 = H, R^3 = Me
23 R^1 = R^2 = All, R^3 = Me
24 R^1 = R^2 = $CH_2CH_2CH_2SCH_2C(O)OMe$, R^3 = Me
25 R^1 = R^2 = $CH_2CH_2CH_2SCH_2C(O)NHCH_2CH_2NH_2$, R^3 = Me
26 R^1 = R^2 = R^3 = All
27 R^1 = R^2 = R^3 = $CH_2CH_2CH_2SCH_2C(O)OMe$
28 R^1 = R^2 = R^3 = $CH_2CH_2CH_2SCH_2C(O)NHCH_2CH_2NH_2$

The experimental verification of the model was undertaken for a fortuitously uncomplicated system, the bacterial AB_5 Shiga-like toxin of *E. coli* 0157. This protein presents all of its ligand binding sites on a nearly flat, radially symmetric, disklike protein built from five identical subunits. When the activities of two sets of radially symmetric ligands with valencies range from 3 to 5 and 6−10 were fitted to thermodynamic model, the activity of a structurally distinct octavalent ligand was accurately predicted.

The most notable achievement of the theory identifies and quantifies an entropic driving force that applies to multivalent systems. This term is not constrained by the loss of conformational entropy that must apply when multiligands tethered through numerous flexible bonds are bound to a receptor.

The model does not treat aggregation and specifically assumes that this does not occur under the conditions of activity measurements. It does not directly address other important aspects of the multivalency that may prevail in different methods of activity measurement when aggregation cannot be avoided or even becomes the driving force for activity enhancement. Conversely, once the microscopic binding parameters are deduced using binding data obtained at appropriate experimental conditions, some of the secondary effects taking place at nonidealized conditions may be predicted by using more elaborate models. Such effects are often the result of high concentration of the receptor and may be corrected by choosing $[R]_{\text{total}}$ at least 100−1000-fold lower than K_{avidity}, although the sensitivity of the assay may suffer.

The $\Delta G_{\text{avidity}}$ notation of eq 10 must correctly represent all thermodynamic parameters of a multivalent interaction such as standard enthalpy and entropy of binding, and in principle, the experimental evidence for the model could have been provided by titration microcalorimetry, one of the most precise and direct techniques for determining these thermodynamic parameters. However, in the case of the multivalent interactions at play here this approach had several drawbacks. The relatively high reagent concentrations needed to generate sufficient heat are expected to and, in fact, do result in extensive cross-linking between the ligand and several copies of the multivalent receptor.[11,15b] Under these conditions, the original balance between bound and unbound receptor species may be disturbed by extensive aggregation. Additionally, the signal produced in a microcalorimetry experiment is proportional to the number of binding sites engaged rather than to the concentration of free receptor,

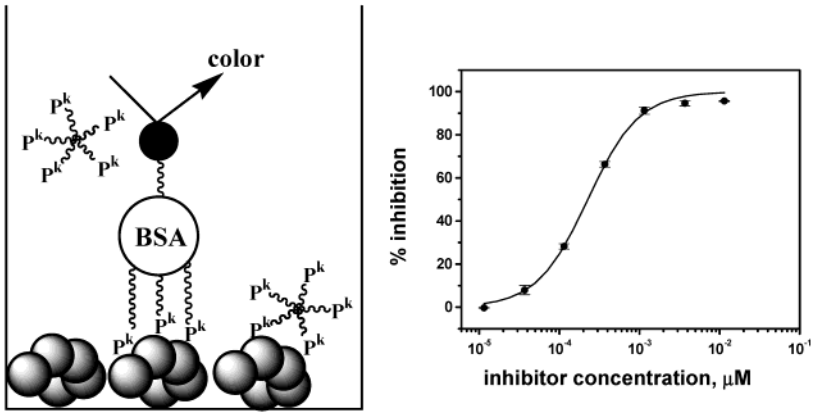

Figure 6. Schematic of ELISA and representative inhibition isotherm. An inhibitor and a reporter molecule compete for binding to an immobilized receptor. Experimental data points for compound **9** with vertical bars designating standard deviation for triplicate measurements. Sigmoidal curve fitting is used for finding IC_{50}.

Table 1. Activities of Synthetic SLT-1 Inhibitors

cmpd	$1/IC_{50}$ (M^{-1})[a]	cmpd	$1/IC_{50}$ (M^{-1})[a]
1	4.7×10^2	**6** predicted	1.26×10^9
2	1.8×10^4	**6** measured	1.4×10^9
3	2.8×10^5	**7**	2.1×10^7
4	2.8×10^6	**8**	5.9×10^8
5	4.1×10^7	**9**	5.0×10^9

[a] Standard deviations of fitting do not exceed 10%.

Table 2. Microscopic Thermodynamic Parameters for a Series of Univalently Branched Inhibitors **3**−**5** and a Series of Bivalently Branched Inhibitors **7**−**9**

cmpds	ΔG°_{inter}	ΔG°_{intra}	χ^2
3−**5**	−2.61	−1.13	0.01
7−**9**	−4.94	−1.33	0.009

which is a crucial parameter in our model. Consequently, conventional solid-phase assays that are less likely to cause aggregation, since they are run under nanomolar concentrations of receptor, were employed in this study.

A unique and essential feature of our thermodynamic model is its reliance on the measurement of the concentration of free multimeric receptor, a quantity that is usually not easily accessible. The signal generated in an assay must be linearly proportional to concentration of bound or unbound receptor over a wide range of ligand concentrations to afford data for a binding isotherm that is suitable for this thermodynamic analysis. We accomplish this objective by a solid-phase assay in which the size of the reporter molecule, biotinylated P^k-BSA glycoconjugate (globular protein MW ≈ 70 000), approximates that of the B_5 receptor (an essentially globular protein, MW ≈ 75 000). When these molecules interact, it is no longer possible for our multivalent ligand to bind a B_5 receptor that has even some of its receptor sites bound to a single reporter group. Thus, the signal generated by the biotinylated P^k-BSA reporter molecule is proportional to the concentration of free receptors. This solid-phase assay also functions at concentrations that approach those of physiological systems.

The dependence of avidity on the density and arrangement of binding sites on the surface was previously observed in other systems.[21] The receptor integrity as a multivalent unit has to be preserved upon immobilization; the signal-generating reporting

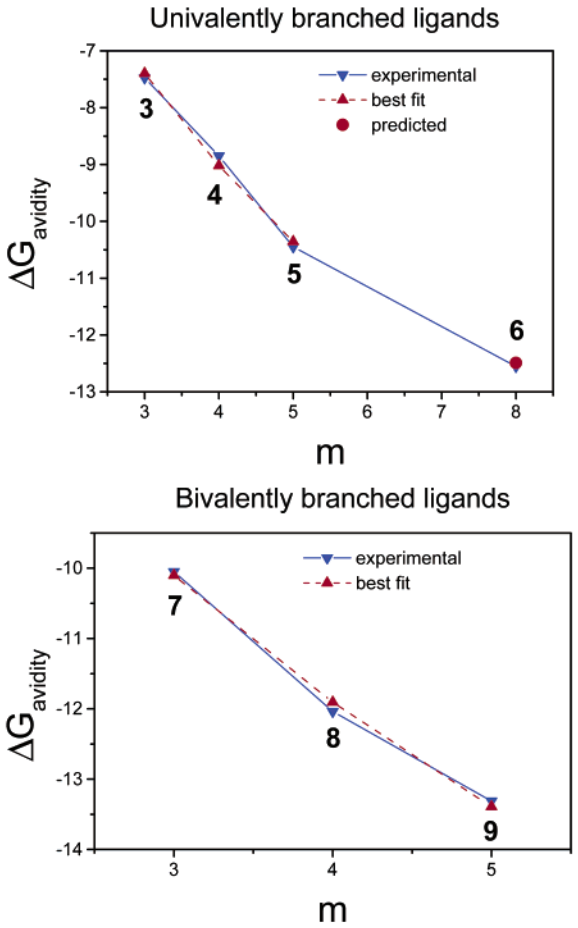

Figure 7. Result of nonlinear fitting of binding data with the thermodynamic model. Microscopic binding parameters ΔG°_{inter} and ΔG°_{intra} found by χ^2 minimization were used to calculate theoretical values of IC_{50} according to eq 9 or 10. Data points are connected only for demonstration purposes to emphasize the tendencies.

molecule should preferably bind to the whole multivalent receptor rather than to smaller or bigger subsets of the randomly distributed binding sites.

When competitive interaction takes place

$$R + L \rightleftharpoons RL$$
$$R + I \rightleftharpoons RI \qquad (19)$$

where L is the ligand of interest and I is indicator, at $[L]_o >$

(21) Feldman, R. G.; Hamel, M. E.; Breukels, M. A.; Concepcion, N. F.; Anthony, B. F. *J. Immunol. Methods* **1994**, *170* (1), 37−45.

$[R]_o$ and $[I]_o > [R]_o$, the relationship between [L] at midpoint of binding isotherm, IC_{50}, and binding constant K_L depends on the coupled interaction between receptor and indicator as follows (see Supporting Information):

$$IC_{50} = \frac{1 + K_I[I]}{K_L} \tag{20}$$

Consequently, the inhibition assay always underestimates the activity of the inhibitor.[22,23] The extent of underestimation depends on the product of the concentration of indicator and binding constant for the interaction between receptor and indicator, $K_I[I]$. In this work, the value of this product was chosen to be equal to unity to obtain sufficient signal. Hence, all measured $K_{avidity}$ values contain a systematic error, namely, a factor of 2. In energy terms, this translates into a systematic error of −0.41 kcal/mol in the values for ΔG°_{inter}.

After correction, ΔG°_{inter} for the series of univalently branched ligands **3**−**6** becomes −3.02 kcal/mol, and for the series of bivalently branched ligands **7**−**9** ΔG°_{inter} is −5.35 kcal/mol. It is instructive to compare these values with activities of the monovalent analogues of each branch, ligands **1** and **2** (Scheme 1).

The no-aggregation condition can by no means be maintained in the case of small ligands since there is no steric hindrance to prevent several molecules of **1** or **2** from binding to the same oligomeric protein. The result of such indiscriminate random binding is the characteristic distribution of "aggregated" bound states as we have recently shown by FTICR mass-spectrometry.[15b] This distribution leads, in competitive inhibition assay, to apparent overestimation of a small ligand activity according to the following expression

$$IC_{50} = \frac{\sqrt[n]{2 + K_I[I]} - 1}{K_L} \tag{21}$$

where $n = 5$ is the number of binding sites per protein oligomer.

Taking into account that, in our case, $K_I[I] = 1$, the magnitude of $1/IC_{50}$ overestimates activities of **1** and **2** by a factor of 4. After this dual adjustment, the free binding energies 1 (−2.84 kcal/mol) and 2 (−5.01 kcal/mol) agree well with the corresponding ΔG°_{inter} values for corresponding series of multivalent ligands.

Surprisingly, the difference between uni- and bivalently branched ligands appears to be much less pronounced with respect to intramolecular interaction ($\Delta\Delta G^\circ_{intra} = -0.2$ kcal/mol). This should be attributed to different effective concentrations that can be achieved by a pendant ligand at the site of binding due to different spatial requirements for the effective length of tethers in the two series.[8] This may indicate a less than optimal length of tether used in the series of bivalent ligands. Further synthetic efforts as well as extensive molecular dynamics simulations[8] are required to address this issue.

On the basis of obtained ΔG°_{intra} values the contribution of the free energy term and the avidity entropy term to avidity can be calculated (Table 3). The approximate parity between these two terms does not permit us to attribute avidity enhancement to only one factor in this case study. The binding is driven by both intramolecular free energy and avidity entropy. The data illustrate the importance of the avidity entropy term in determining the high avidity of STARFISH type inhibitors, notwithstanding the almost prohibitive number of torsional degrees of freedom and associated loss of conformational entropy when an inhibitor with so many single bonds is bound. As noted earlier, the latter can only detract from the magnitude of ΔG°_{intra}, but the avidity entropy is unaffected and is determined by the permutations of branches of multivalent ligand and receptor sites.

Table 3. Contributions of the Intramolecular Energy Term and Avidity Entropy Term to $\Delta G^\circ_{avidity}$ from Eq 10 for Multivalent Ligands **3**−**9**

cmpd	$\Sigma w_i(i-1)\Delta G^\circ_{intra}$	$-T\Delta S^\circ_{avidity}$[a]
3	−2.10	−2.68
4	−3.10	−3.32
5	−3.92	−3.83
6	−4.32	−5.56
7	−2.52	−2.64
8	−3.73	−3.23
9	−4.77	−3.68

[a] kcal/mol.

Dissection of the multivalency effect into elementary thermodynamic parameters provides a basis for computer-assisted rational design of powerful inhibitors. Thus, the relation between ΔG°_{inter} and ΔG°_{intra} suggests the possibility for optimization of tether length to maximize ΔG°_{intra}.[8] Furthermore, knowledge of the microscopic binding parameters, particularly ΔG°_{intra} and calculated Ω_i, affords otherwise unavailable information about the distribution of bound states and offers a new insight into the nature of multivalent interactions.

Notwithstanding the overall increase of binding energy, the statistical effect favors mostly those bound states with low saturation of binding sites of the receptor, whereas the system entropically resists the complete saturation of binding sites. Two examples of such distribution are shown in Figure 8. Three extra branches of the multivalent ligand **6** do not interact with the receptor in a common sense; however, they increase the *probability* of the interaction. Although unable to specifically interact with the receptor, the extra branches of this ligand secure a higher degree of inhibition, increasing the fraction of completely saturated receptor from 54% in a complex with pentavalent ligand **5** to 84% in case of **6**.

In a situation when it is necessarily to inhibit all binding sites to achieve a desirable effect, the fraction of uninhibited bonding sites can be precisely controlled by choosing the appropriate number of branches for assembly of a multivalent inhibitor.

Conclusions

A rigorous thermodynamic model is proposed for the analysis of interactions between multivalent ligands and multivalent receptors in dilute solutions. The model is validated by competitive inhibition assay data for two series of oligovalent ligands. Avidity binding energy is considered to consist of three major elements: (a) intrinsic free binding energy of initial bimolecular reaction of anchoring to a receptor by single branch of a ligand, (b) intrinsic free binding energy for intramolecular binding of ligand branches to the remaining binding sites on the receptor surface, and (c) a combinatorial factor reflecting

(22) (a) Vorberg, E.; Bundle, D. R. *J. Immunol. Methods* **1990**, *132*, 81−9. (b) Sigurskjold, B. W.; Altman, E.; Bundle, D. R. *Eur. J. Biochem.* **1991**, *197*, 239−246.

(23) Chang, K.-J.; Jacobs, S.; Cuatrecasas, P. *Biochim. Biophys. Acta* **1975**, *406*, 294−303.

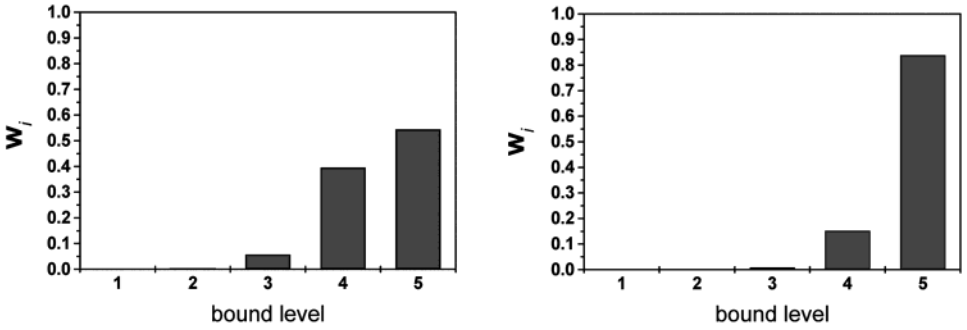

Figure 8. Calculated distribution of bound levels for monovalently branched inhibitors **5** (left panel), **6** (right panel). Number of a bound level indicates number of occupied binding sites in each complex.

the probability of association and dissociation of individual branches. The latter two are major determinants of the free energy increase of a multivalent association with respect to the corresponding monovalent binding.

This treatment of multivalency not only provides a sound appreciation of the principles underlying the avidity gains observed for multivalent ligands that are tailored to match the spacing between binding sites of the AB_5 toxins, it may in principle also be applied to any multivalent ligand−receptor pair with any topology of binding sites. Radially symmetric ligand−receptor combinations will always provide the most favorable avidity entropy gains. Furthermore, it is of interest that proteins with this structural motif are not limited to the bacterial toxins. An important example is mammalian pentraxins that include but are not limited to the acute phase C-reactive protein.[24]

Although the model was developed to describe the *binding* between multivalent ligand and receptor, the prediction of the distribution of bound states provides valuable insight into the *inhibition* of multivalent receptor by a multivalent ligand in situations, when incomplete saturation of receptor binding sites may play a role.

Finally, the ability to access $\Delta G^{\circ}_{\text{intra}}$ when combined with computational approaches to optimize tether length opens up the possibility for computer-assisted rational design of multivalent inhibitors.

Experimental Section

General Methods. Optical rotations were measured on a Perkin-Elmer 241 polarimeter for samples in a 10 cm cell at ambient temperature (22 ± 2 °C). Analytical TLC was performed on silica gel 60-F_{254} (Merck) with detection by quenching of fluorescence and/or by charring with 10% H_2SO_4 in ethanol solution followed by heating at 180 °C. Column chromatography was performed on silica gel 60 (Merck, 40−60 μm), and solvents were distilled prior to use. Sep-Pak C_{18} cartridges (Waters) were conditioned prior to use by washing with methanol (10 mL) and water (20 mL). The ^{1}H NMR spectra were recorded at 500 and 600 MHz (Varian) in $CDCl_3$ (referenced to residual $CHCl_3$ at δ_H 7.24 ppm), CD_3OD (referenced to residual CD_2HOD at δ_H 3.3 ppm), or in D_2O (referenced to internal acetone at δ_H 2.225 ppm). All commercial reagents were used as supplied; solvents were distilled from appropriate desiccants prior to use. After extraction, solutions in DCM were filtered through a cotton plug.

Methyl 4-*O*-{2-*O*-[2-(8-Aminooctylaminocarbonyl)ethyl]-3,6-di-*O*-benzyl-4-*O*-(2,3,4,6-tetra-*O*-benzyl-α-D-galactopyranosyl)-*β*-D-galactopyranosyl}-2,3,6-tri-*O*-benzyl-*β*-D-glucopyranoside (11). A solution of **10**[19] (249 mg, 0.16 mmol) in THF (3 mL) was added dropwise to a solution of 1,8-diaminooctane (116 mg, 0.81 mmol) in THF (5 mL). After 15 min the mixture was taken up in DCM, washed with water, and concentrated. Column chromatography of the residue on silica gel with DCM−MeOH−aq NH_3 (900:100:4 to 800:200:4) gave **11** (232 mg, 92%), $[\alpha]_D$ +27.7°(*c* 0.5; $CHCl_3$); ^{1}H NMR ($CDCl_3$): δ 7.4−7.1 (m, 45 H, arom), 5.38 (t, 1 H, $J_{NH,CH}$ 5.8 Hz, NH), 5.04−5.0 (m, 2 H, H-1″, Bn), 4.84−4.62 (m, 9 H, Bn), 4.51−4.42 (m, 4 H, Bn), 4.38−3.70 (m, 18 H, H-1, H-4, H-6a, H-6b, H-1′, H-4′, H-2″, H-3″, H-4″, H-5″, CH_2O, Bn), 3.52 (s, 3 H, OMe), 3.57−3.06 (m, 10 H, H-2, H-3, H-5, H-2′, H-3′, H-5′, H-6′a, H-6′b, H-6″a, H-6″b), 2.90−278 (m, 2 H, $CH_2NC(O)$), 2.69 (t, 2 H, ^2J 7.1 Hz, CH_2NH_2), 1.50−1.40 (m, 2 H, $C\underline{H}_2CH_2NHCO$), 1.30−1.10 (m, 10 H, $C\underline{H}_2$). Anal. Calcd for $C_{93}H_{110}N_2O_{18}$·0.5 H_2O: C, 71.93; H, 7.20; N, 1.80. Found C, 71.98; H, 7.21; N, 1.82.

Methyl 4-*O*-{2-*O*-[2-(8-Aminooctylaminocarbonyl)ethyl]-4-*O*-(α-D-galactopyranosyl)-*β*-D-galactopyranosyl}-*β*-D-glucopyranoside (12). A solution of **11** (216 mg, 0.14 mmol) in HOAc (10 mL) was hydrogenated at in the presence of 10% Pd/C (20 mg). The mixture was filtered and concentrated, and a solution of the residue in water was passed through Sep-Pak (C-18) cartridge and eluted with H_2O−MeOH (1:0 to 7:3) to give **12** (106.2 mg, 96%), $[\alpha]_D$ +38.5°(*c* 0.3; H_2O); ^{1}H NMR (D_2O): δ 4.92(d, 1 H, $J_{1'',2''}$ 3.8 Hz, H-1″), 4.53 (d, 1 H, $J_{1',2'}$ 7.7 Hz, H-1′), 4.37 (d, 1 H, $J_{1,2}$ 8.1 Hz, H-1), 4.33 (d, 1 H, $J_{5'',6''a} \sim J_{5'',6''b} \sim$ 6.4 Hz, H-5″), 4.22−4.16 (m, 2 H, OCH_2), 4.07−3.99 (m, 4 H, H-4′, H-4″, H-6a, OCH_2), 3.94−3.88 (m, 3 H, H-3″, H-6″a, OCH_2), 3.86−3.80 (m, 3 H, H-6b, H-6′a, H-2″), 3.76−3.70 (m 4 H, H-3′, H-5′, H-6′b, H-6″b), 3.66 (t, 1 H, $J_{3,4}$ 9.3 Hz, H-4), 3.62 (t, 1 H, $J_{2,3}$ 10.1 Hz, H-3), 3.57 (s, 3 H, OMe), 3.54 (ddd, 1 H, $J_{4,5}$ 1.8 Hz, $J_{5,6a}$ 5.1 Hz, $J_{5,6b}$ 7.3 Hz, H-5), 3.42 (broad t, 1 H, $J_{2',3'}$ 8.4 Hz, H-2′), 3.30 (broad t, 1 H, $J_{2,3}$ 9.1, H-2), 3.11 (t, 2 H, ^3J 6.8 Hz, C(O)-$NHC\underline{H}_2$), 2.98 (t, 2 H, ^3J 7.5 Hz, CH_2NH_2), 1.91 (s, 3 H, Ac), 1.63 (m, 2 H, $C\underline{H}_2CH_2NH_2$), 1.50 (m, 2 H, $C(O)NHCH_2C\underline{H}_2$), 1.40−1.30 (m, 8 H, CH_2). Electrospray ionization MS for $C_{30}H_{57}N_2O_{18}$ calcd 733.3606, found 733.3601.

Methyl 4-*O*-{2-*O*-{2-[8-(4-Ethoxy-2,3-dioxo-3-cyclobutenylamino)octyl]carbamoyloxyethyl}-4-*O*-(α-D-galactopyranosyl)-*β*-D-galactopyranosyl}-*β*-D-glucopyranoside (13). To a solution of **12** (101 mg, 127 μmol) in MeOH (4 mL) were added 3,4-diethoxy-3-cyclobuten-1,2-dion (43.4 mg, 254 μmol) and Et_3N (20 mg, 205 μmol). After 3 h the mixture was concentrated. The residue was chromatographed on Sep-Pak (C-18) in water−MeOH (9:1 to 6:4) to give **13** (94.5 mg, 87%), $[\alpha]_D$ +37.5 °(*c* 0.6; H_2O); ^{1}H NMR (D_2O): δ 4.97 (d, 1 H, $J_{1'',2''}$ 4.0 Hz, H-1″), 4.76−4.69 (m, 2 H, $OC\underline{H}_2CH_3$), 4.52 (d, 1 H, $J_{1',2'}$ 7.8 Hz, H-1′), 4.36 (d, 1 H, $J_{1,2}$ 8.1 Hz, H-1), 4.35 (d, 1 H, $J_{5'',6''a} \sim J_{5'',6''b} \sim$ 6.4 Hz, H-5″), 4.24−4.16 (m, 2 H, OCH_2), 4.06−3.99 (m, 4 H, H-4′, H-4″, H-6a, OCH_2), 3.95−3.90 (m, 3 H, H-3″, H-6″a, OCH_2), 3.86−3.80 (m, 3 H, H-6b, H-6′a, H-2″), 3.78−3.69 (m 4 H, H-3′, H-5′, H-6′b, H-6″b), 3.66 (t, 1 H, $J_{3,4}$ 9.3 Hz, H-4), 3.62 (t, 1 H, $J_{2,3}$ 9.1 Hz, H-3), 3.60 (t, 1 H, ^3J 6.8 Hz, $C\underline{H}_2NHSQ$, rotamer a), 3.57 (s, 3 H, OMe), 3.54 (ddd, 1 H, $J_{4,5}$ 2.0 Hz, $J_{5,6a}$ 5.3 Hz, $J_{5,6b}$ 7.3 Hz, H-5), 3.47

(24) Gewurz, H.; Zhang, X.-H.; Lint, T. F. *Curr. Opin. Immun.* **1995**, *7*, 54−64.

(t, 1 H, ^3J 6.8 Hz, CH_2NHSQ, rotamer b), 3.42 (broad dd, 1 H, $J_{2',3'}$ 9.6 Hz, H-2′), 3.30 (t, 1 H, $J_{2,3}$ 8.4, H-2), 3.10 (broad t, 2 H, ^3J 6.6 Hz, C(O)NHCH_2), 1.61 (m, 2 H, CH_2CH_2NH), 1.50−1.42 (m, 5 H, C(O)-NHCH$_2$CH_2, OCH$_2$CH_3), 1.34−1.28 (m, 8 H, CH_2). Electrospray ionization MS for $C_{36}H_{60}N_2O_{21}Na$ calcd 879.3586, found 879.3606.

2-Hydroxy-1,3-bis-{{methyl-4-*O*-[3,6-di-*O*-benzyl-4-*O*-(2,3,4,6-tetra-*O*-benzyl-α-D-galactopyranosyl)-*β*-D-galactopyranosyl]-2,3,6-tri-*O*-benzyl-*β*-D-glucopyranoside}-2′-yloxyethyl}oxycarbonylaminopropane (14). A solution of **10** (643 mg, 0.418 mmol) and 1,3-diamino-2-hydroxypropane (18.8 mg, 0.209 mmol) in THF (10 mL) was stirred overnight at room temperature. The mixture was concentrated and chromatographed on silica gel in hexanes−ethyl acetate (7:3, then 3:2) to give **14** (554 mg, 92.3%), $[\alpha]_D$ +27.2°(*c* 0.6; $CHCl_3$); ^{1}H NMR ($CDCl_3$): δ 7.4−7.1 (m, 90 H, arom), 5.72 (m, 2 H, NH), 5.05−5.00 (m, 4 H, H-1″, Bn), 4.82 (d, 2 H, ^2J 11.3 Hz, Bn), 4.79 (d, 2 H, ^2J 11.0 Hz, Bn), 4.74−4.60 (m, 16 H, OCH_2, Bn), 4.50−4.24 (m, 22 H, H-1, H-1′, H-4′, Bn), 4.13−3.73 (m, 24 H, H-4, H-6a, H-6b, H-5′, H-6′a, H-2″, H-3″, H-4″, H-5″, OCH_2, Bn), 3.52 (t, 2 H, $J_{2,3} \sim J_{3,4}$ 9.1 Hz, H-3), 3.51 (s, 6 H, Me), 3.50−3.22 (m, 13 H, H-2, H-5, H-2′, H-6′b, H-6″a, H-6″b, CHCH$_2$N), 3.13 (dd, 2 H, $J_{2',3'}$ 8.1 Hz, $J_{3',4'}$ 4.7 Hz, H-3′), 2.90−2.60 (m, 4 H, CH_2N). Anal. Calcd for $C_{173}H_{190}N_2O_{37}$: C, 71.91; H, 6.63; N, 0.97. Found C, 71.82; H, 6.71; N, 0.95.

1,3-bis-{{Methyl 4-*O*-[3,6-di-*O*-benzyl-4-*O*-(2,3,4,6-tetra-*O*-benzyl-α-D-galactopyranosyl)-*β*-D-galactopyranosyl]-2,3,6-tri-*O*-benzyl-*β*-D-glucopyranoside}-2′-yloxyethyl}oxycarbonylamino-2-(4-nitrophenyloxy)carbonyloxypropane (15). A solution of **14** (552 mg, 0.191 mmol) and 4-nitrophenyl chloroformate (46 mg, 0.228 mmol) in dry pyridine was stirred overnight at 30 °C. Pyridine was removed by evaporation and coevaporation with toluene twice. Chromatography of the residue on silica gel with pentane−ethyl acetate (80:20, 60:40) gave **15** (374 mg, 75%), $[\alpha]_D$ +33.6°(*c* 0.6; $CHCl_3$); ^{1}H NMR ($CDCl_3$): δ 8.1 (d, 2 H, ^3J 9.0 Hz, $C_6H_4NO_2$), 7.4−7.1 (m, 92 H, arom), 5.93 (m, 2 H, NH), 5.05−5.00 (m, 4 H, H-1″, Bn), 4.82 (d, 2 H, ^2J 11.9 Hz, Bn), 4.77−4.56 (m, 16 H, Bn), 4.49−3.71 (m, 47 H, H-1, H-4, H-6a, H-6b, H-1′, H-4′, H-5′, H-2″, H-3″, H-4″, H-5″, OCH_2, CHCH$_2$N, Bn), 3.51 (s, 6 H, Me), 3.52−3.11 (m, 18 H, H-2, H-3, H-5, H-2′, H-3′, H-6′a, H-6′b, H-6″a, H-6″b, CH_2N), 2.81−2.66 (m, 2 H, CH_2N). Anal. Calcd for $C_{180}H_{193}N_3O_{41}$: C, 70.78; H, 6.37; N, 1.38. Found C, 70.74; H, 6.34; N, 1.36.

1,3-Bis-{{methyl 4-*O*-[3,6-di-*O*-benzyl-4-*O*-(2,3,4,6-tetra-*O*-benzyl-α-D-galactopyranosyl)-*β*-D-galactopyranosyl]-2,3,6-tri-*O*-benzyl-*β*-D-glucopyranoside}-2′-yloxyethyl}oxycarbonylamino-2-(8-aminooctyl)carbamoyloxypropane (16). A solution of **15** (350 mg, 0.115 mmol) in THF (2 mL) was added dropwise to a solution of 1,8-diaminooctane (315 mg, 1.49 mmol) in THF (1.5 mL). After 15 min TLC (DCM:MeOH, 10:1) indicated that the reaction completed. Concentration of the reaction mixture and column chromatography of the residue on silica gel with DCM−MeOH−aq NH_3 (10:1:0.1) gave **16** (348 mg, 98%), $[\alpha]_D$ +28.6°(*c* 0.6; $CHCl_3$); ^{1}H NMR (CD_3OD − $CDCl_3$): δ 7.4−7.1 (m, 90 H, arom), 5.09 (d, 2 H, ^2J 11.0 Hz, Bn), 5.04 (d, 2 H, $J_{1'',2''}$ 2.4 Hz, H-1″), 4.8−4.55 (m, 12 H, Bn), 4.52−4.03 (m, 32 H, H-1, H-1′, CHCH$_2$N, CH_2NH, CH_2O, Bn), 3.96−3.78 (m, 23 H, H-4, H-6a, H-6b, H-4′, H-5′, H-2″, H-3″, H-4″, H-5″, CH, CH_2O), 3.61 (m, 2 H, H-6′a), 3.51 (s, 6 H, OMe), 3.54−3.06 (m, 18 H, H-2, H-3, H-5, H-2′, H-3′, H-6′b, H-6″a, H-6″b, CH_2N), 3.00−2.95 (m, 2 H, CH_2N), 2.79 (t, 2 H, ^2J 7.6 Hz, CH_2NH_2), 1.67 (p, 2 H, ^3J 6.2 Hz, CH$_2$CH$_2$NHCO), 1.57−1.52 (m, 1 H, CH$_2$CH$_2$NH$_2$), 1.46−1.20 (m, 7 H, CH_2), 0.90−0.83 (m, 2 H, CH_2). Anal. Calcd for $C_{182}H_{208}N_4O_{38}$: C, 71.45; H, 6.85; N, 1.83. Found C, 71.36; H, 6.91; N, 1.63.

1,3-Bis-{{methyl-4-*O*-[4-*O*-(α-D-galactopyranosyl)-*β*-D-galactopyranosyl]-*β*-D-glucopyranoside}-2′-yloxyethyl}oxycarbonylamino-2-(8-aminooctyl)carbamoyloxypropane Acetic Acid Salt (17). A solution of **16** (350 mg, 0.114 mmol) in HOAc (10 mL) was hydrogenated at in the presence of 10% Pd/C (20 mg). The mixture was filtered and concentrated, and a solution of the residue in water was applied onto Sep-Pak (C-18) cartridge and eluted with MeOH−H_2O (3:7) to give **17** (125 mg, 69%), $[\alpha]_D$ +38.2°(*c* 0.17; H_2O); ^{1}H NMR (D_2O): δ 4.92 (d, 2 H, $J_{1'',2''}$ 3.5 Hz, H-1″), 4.8 (m, under HOD, 1 H, CH), 4.48 (m, 4 lines, 2 H, H-1′), 4.37−4.29 (m, 4 H, H-1, H-5″), 4.22−4.16 (m, 4 H, CH_2O), 4.10−3.50 (m, broad lines, 36 H, H-3, H-4, H-5, H-6a, H-6b, H-3′, H-4′, H-5′, H-6′a, H-6′b, H-2″, H-3″, H-4″, H-6″a, H-6″b, CH_2O, CH_2N), 3.54 (s, 6 H, OMe), 3.37 (broad t, 2 H, $J_{2',3'}$ 9.1 Hz, H-2′), 3.26 (broad t, 2 H, $J_{2,3}$ 8.2, H-2), 3.4−3.2 (m, 4 H, CH_2NH), 3.06 (t, 2 H, ^3J 6.7 Hz, C(O)NHCH_2), 2.95 (t, 2 H, ^3J 7.6 Hz, CH_2NH_2), 1.87 (s, 3 H, Ac), 1.63 (m, 2 H, CH_2CH$_2$NH$_2$), 1.50−1.20 (m, 8 H, CH_2). Electrospray ionization MS for $C_{56}H_{101}N_4O_{38}$ calcd 1437.6094, found 1437.6133.

1,3-Bis-{{methyl-4-*O*-[4-*O*-(α-D-galactopyranosyl)-*β*-D-galactopyranosyl]-*β*-D-glucopyranoside}-2′-yloxyethyl}oxycarbonylamino-2-[8-(4-ethoxy-2,3-dioxo-3-cyclobutenylamino)octyl]carbamoyloxypropane (18). To a solution of **17** (30.8 mg, 20.5 μmol) in 1 mL of MeOH 3,4-diethoxy-3-cyclobuten-1,2-dion (7 mg, 41 μmol) and Et_3N (4 mg, 41 μmol) were added. After 3 h the mixture was concentrated. The residue was chromatographed on Sep-Pak (C-18) in water−MeOH (9:1 to 7:3) to give **18** (26.8 mg, 84%), $[\alpha]_D$ +50.7 °(*c* 0.14; H_2O); ^{1}H NMR (D_2O): δ 4.96 (d, 2 H, $J_{1'',2''}$ 3.9 Hz, H-1″), 4.8 (m, under HOD, 3 H, CH, OCH_2CH$_3$), 4.52 (m, 4 lines, 2 H, H-1′), 4.38 (m, 2 H, H-1), 4.34 (broad t, 2 H, $J_{5'',6''a} \sim J_{5'',6''b} \sim$ 6.1 Hz, H-5″), 4.25−4.16 (m, 4 H, OCH_2), 4.07−4.00 (m, 8 H, H-4′, H-4″, H-6a, OCH_2), 3.94−3.88 (m, 6 H, H-3″, H-6″a, CH_2), 3.86−3.70 (m, 14 H, H-6b, H-2″, H-3′, H-5′, H-6′a, H-6′b, H-6″b), 3.66−3.54 (m, 13 H, H-3, H-4, H-5, OMe, CH_2NHSQ rotamer a), 3.49 (t, 1 H, ^3J 6.9 Hz CH_2NHSQ rotamer b), 3.41 (broad t, 2 H, H-2′), 3.40−3.28 (m, 6 H, H-2, CH_2NH), 3.10 (t, 2 H, ^3J 6.5 Hz, C(O)NHCH_2), 1.62 (m, 2 H, CH_2CH$_2$NHSQ), 1.45 (t, 3H, ^3J 7.2 Hz, CH_2CH_3), 1.50−1.30 (m, 10 H, CH_2). Electrospray ionization MS for $C_{62}H_{105}N_4O_{41}$ calcd 1561.6254, found 1561.6253.

Methyl 2,3,4-tri-*O*-allyl-*β*-D-glucopyranoside (20). To a solution of **19**[25] (1.65 g, 3.78 mmol) in dry DMF (15 mL) NaH (95%, 310 mg) and allyl bromide (1.1 mL) were added. The mixture was stirred for 2 h then the reaction was quenched with MeOH, diluted with ethyl acetate, and washed with brine and concentrated. The residue was dissolved in aq TFA (90%, 5 mL) and stirred for 1 h then concentrated, coevaporated with toluene and chromatographed on silica gel with hexane−ethyl acetate (70:30 to 60:40) to give **20** (860 mg, 72%). $[\alpha]_D$ −1.6°(*c* 1.2; $CHCl_3$); ^{1}H NMR ($CDCl_3$): δ 5.97−5.86 (m, 3 H, All), 5.28−5.13 (m, 6 H, All), 4.35−4.28 (m, 3 H, All), 4.26−4.22 (m, 1 H, All), 4.22 (d, 1 H, $J_{1,2}$ 7.7 Hz, H-1), 4.16−4.10 (m, 2 H, All), 3.87−3.84 (m, 1 H, H-6a), 3.73−3.68 (m, 1 H, H-6b), 3.56 (s, 3 H, Me), 3.39 (t, 1 H, $J_{3,4} \sim J_{3,2} = 9.0$ Hz, H-3), 3.33 (t, 1 H, $J_{3,4} \sim J_{4,5}$ 9.0 Hz, H-4), 3.28−3.25 (m, 1 H, H-5), 3.14 (dd, 1 H, H-2). Calcd for $C_{16}H_{26}O_6$: C, 61.13, H, 8.34. Found C, 61.05; H, 8.54.

Methyl 2,3,4-tri-*O*-(5-methoxycarbonyl-4-thia-pentyl)-*β*-D-glucopyranoside (21). A solution of **20** (426 mg, 1.35 mmol) in neat methyl thioglycolate (3 mL) was irradiated with UV 254 nm for 3 h then chromatographed on silica gel with hexane−ethyl acetate (7:3 to 2:3) to give **21** (712 mg, 83%). $[\alpha]_D$ −5.4°(*c* 1.1; $CHCl_3$); ^{1}H NMR ($CDCl_3$): δ 4.15 (d, 1 H, $J_{1,2}$ 7.9 Hz, H-1), 3.86−3.80 (m, 4 H, H-6a, CH_2O) 3.71 (s, 9 H, Me), 3.76−3.60 (m, 4H, H-6b, CH_2O), 3.50 (s, 3 H, Me), 3.21−3.20 (m, 9 H, H-3, H-4, H-5, $CH_2C(O)$), 3.01−2.97 (m, 1 H, H-2), 2.69 (dt, 6 H, $J \sim J$ 7.3 Hz, J 13.9 Hz, CH_2), 1.88−1.78 (m, 6 H, CH_2). Calcd for $C_{25}H_{44}O_{12}S_3$: C, 47.45, H, 7.01; S, 15.20. Found C, 47.20; H, 7.09; S, 15.15.

Methyl 2,3,4-tri-*O*-(9-amino-7-aza-4-thia-non-6-onyl)-*β*-D-glucopyranoside Trifluoroacetic Acid Salt (22). A mixture of **21** (630 mg, mmol) in neat ethylenediamine (5 mL) was stirred for 2 days at 65 °C then concentrated and purified by HPLC on C-18 column with water−MeOH−TFA (80:20:0.1%) to give **22** (480 mg) ^{1}H NMR

(25) MacManus, D. A.; Vulfson, E. N. *Carbohydr. Res.* **1995**, *279*, 281−292.

(D_2O): δ 4.37 (d, 1 H, $J_{1,2}$ 7.9 Hz, H-1), 3.91−3.7.0 (m, 8 H, CH_2O, H-6a, H-6b), 3.58−3.54 (m, 6 H, CH_2N), 3.33 (s, 6 H, CH_2CO), 3.44−3.28 (m, 3 H, H-3, H-4, H-5), 3.18 (t, 6 H, CH_2N), 3.12 (t, 1 H, H-2), 2.71−2.66 (m, 6 H, CH_2S), 1.98−1.86 (m, 6 H, $C\underline{H}_2CH_2S$). Electrospray ionization MS for triamine [M + H] $C_{28}H_{57}N_6O_9S_3$ calcd 717.3349, found 717.3352.

Methyl 2,3,4,6-tetra-*O*-(5-methoxycarbonyl-4-thia-pentyl)-β-D-glucopyranoside (24). A solution of methyl 2,3,4,6-tetra-*O*-allyl-β-D-glucopyranoside **23**[26] (1.52 g, 4.28 mmol) in neat methyl thioglycolate (6 mL) was irradiated with UV 254 for 8 h then concentrated and chromatographed on silica gel with hexane−ethyl acetate (2:1 to 1:1) to give **24** (3.2 g, 95%).$[\alpha]_D$ −5.9°(*c* 0.8; $CHCl_3$); ^{1}H NMR ($CDCl_3$): δ 4.07 (d, 1 H, $J_{1,2}$ 7.9 Hz, H-1), 3.85−3.70 (m, 4 H, CH_2O) 3.72 (s, 2 H, Me), 3.78−3.50 (m, 6 H, H-6a, H-6b, CH_2O), 3.47 (s, 3 H, Me), 3.22−3.17 (m, 11 H, H-3, H-4, H-5, $CH_2C(O)$), 3.01−2.98 (m, 1 H, H-2), 2.72−2.67 (m, 8 H, CH_2), 1.90−1.78 (m, 8 H, CH_2). Anal. Calcd for $C_{31}H_{54}O_{14}S_4$: C, 47.80, H, 6.99; S, 16.46. Found C, 47.73; H, 7.00; S, 16.42.

Methyl 2,3,4,6-tetra-*O*-(9-amino-7-aza-4-thia-non-6-onyl)-β-D-glucopyranoside Trifluoroacetic Acid Salt (25). A mixture of **24** (310 mg, mmol) in neat ethylenediamine (5 mL) was stirred for 2 days at 65 °C then concentrated and purified by HPLC on C-18 column with water−MeOH (80:20) with 0.1% TFA to give **25** (283 mg) ^{1}H NMR (D_2O): δ 4.45 (d, 1 H, $J_{1,2}$ 8.0 Hz, H-1), 3.9−3.6 (m, 10 H, CH_2O, H-6a, H-6b), 3.58−3.54 (m, 8 H, CH_2N), 3.48 (ddd, 1 H, $J_{5,4}$ 0.7 Hz, $J_{5,6a}$ 10.0 Hz, $J_{5,6b}$ 4.4 Hz, H-5), 3.40−3.31 (m, 2H, H-3, H-4), 3.34 (s, 8 H, CH_2CO), 3.17 (t, 8 H, CH_2N), 3.11 (t, 1 H, H-2), 2.70−2.66 (m, 8 H, CH_2S), 1.98−1.85 (m, 8 H, $C\underline{H}_2CH_2S$). Electrospray ionization MS for tetraamine [M + H] $C_{35}H_{71}N_8O_{10}S_4$ calcd 891.4176, found 891.4167.

1,2,3,4,6-Penta-*O*-(5-methoxycarbonyl-4-thio-pentyl)-β-D-glucopyranoside (27). A mixture of 1,2,3,4,6-penta-*O*-allyl-β-D-glucopyranoside **26**[26] (449 mg, 1.18 mmol) and methyl thioglycolate (2.64 mL, 25 equiv) in MeOH (3 mL) was irradiated with UV source at 254 nm for 1 h then concentrated. Chromatography of the residue on silica gel in hexane−ethyl acetate (5:5 to 4:6) gave **27** (545 mg, 51%). ^{1}H NMR ($CDCl_3$): δ 4.12 (d, 1 H, $J_{1,2}$ 7.8 Hz, H-1), 3.90−3.45 (m, 12 H, CH_2O, H-6a, H-6b), 3.67 (s, 15 H, CH_3), 3.17 (s, 10 H, CH_2CO), 3.17−3.11 (m, 3 H, H-3, H-4, H-5), 2.96 (m, 1 H, H-2), 2.68−2.63 (m, 10 H, CH_2S), 1.9−1.75 (m, 10 H, $C\underline{H}_2CH_2S$). Anal. Calcd for $C_{36}H_{62}O_{16}S_5$: C, 47.45; H, 6.86; S, 17.60. Found C, 47.32; H, 6.91; S, 17.58.

1,2,3,4,6-Penta-*O*-(9-amino-7-aza-4-thia-non-6-onyl)-β-D-glucopyranoside Acetic Acid Salt (28). A solution of **27** (170 mg) in neat ethylenediamine (3 mL) was stirred at 60 °C for 2 days, then concentrated and coevaporated with water. A portion of the mixture was applied onto a Biogel P-2 column, the product was eluted with aq 0.01 M AcOH to give pentaamine pentaacetate **28**.^{1}H NMR (D_2O): δ 4.43 (d, 1 H, $J_{1,2}$ 8.9 Hz, H-1), 4.02−3.29 (m, 15 H, CH_2O, H-3, H-4, H-5, H-6a, H-6b), 3.54 (t, 10 H, ^3J = 6.1 Hz, CH_2N), 3.34 (s, 10 H, CH_2CO), 3.14 (t, 10 H, CH_2N), 3.19−3.09 (m, 1 H, H-2), 2.73−2.66 (m, 10 H, CH_2S), 1.98−1.85 (m, 25 H, CH_2CH_2S, Ac). Electrospray ionization MS for pentaamine [M + H] $C_{41}H_{83}N_{10}O_{11}S_5$ calcd 1051.4846, found 1051.4833.

General Procedure for Preparation of P^k-trisaccharide Dendrimers 3−9. A solution of a mixture of tri-, tetra- or pentaamino derivative (**22**, **25**, or **28**) with a squaric acid derivative **13** or **18** (1.5 equiv per NH_2 group) in borate buffer (pH 9) was stirred for 24 h at 40 °C. A HPLC purification of the reaction mixture using reversed phase column C-18 with UV detection at 300 nm in gradient water−MeOH (100:0 to 30:70) afforded title compounds with 70−80% yield.

Multivalent ligand 3: deconvolution of multiple charged ions in electrospray ionization MS for $C_{130}H_{218}N_{12}O_{69}S_3$ calcd[28] 3149.36, found 3149, MALDI TOF found 3146.

Multivalent ligand 4: deconvolution of multiple charged ions in electrospray ionization MS for $C_{171}H_{286}N_{16}O_{90}S_4$ calcd[28] 4134.42, found 4134, MALDI TOF found 4136.

Multivalent ligand 5: deconvolution of multiple charged ions in electrospray ionization MS for $C_{211}H_{352}N_{20}O_{111}S_5$ calcd[28] 5105.45, found 5105, MALDI TOF found 5123.

Multivalent ligand 6: MALDI TOF for $C_{334}H_{560}N_{42}O_{172}$ calcd[28] 7916.20, found found 7938.

Multivalent ligand 7: deconvolution of multiple charged ions in electrospray ionization MS for $C_{208}H_{350}N_{18}O_{129}S_3$ calcd[28] 5263.25, found 5264, MALDI TOF found 5274.

Multivalent ligand 8: deconvolution of multiple charged ions in electrospray ionization MS for $C_{275}H_{462}N_{24}O_{170}S_4$ calcd[28] 6952.93, found 6953.

Multivalent ligand 9: deconvolution of multiple charged ions in electrospray ionization MS for $C_{341}H_{572}N_{30}O_{211}S_5$ calcd[28] 8628.60, found 8630, MALDI TOF found 8660.

Acknowledgment. We are grateful to Ms. Joanna Sadowska for performing solid-phase assays and Dr. E. N. Kitova for obtaining mass spectrometry data. The studies were supported by a grant from the Canadian Bacterial Diseases Network (CBDN).

Supporting Information Available: Detailed derivation of eqs 10, 17, 20, and 21, MAPLE program for nonlinear fitting of binding data to thermodynamic model, ^{1}H NMR spectra for multivalent ligands **3**−**9**, FTICR mass spectrum for STARFISH inhibitor **9** (PDF). This material is available free of charge via the Internet at http://pubs.acs.org.

JA038223N

(26) Lakhmiri, R.; Lhoste, P.; Sinou, D. *Synth. Commun*. **1990**, *20*, 1551−1554.

(27) Kieburg, C.; Dubber, M.; Lindhorst, T. K. *Synth. Lett.* **1997**, *12*, 1447−1449.

(28) Calculated molecular weight. Due to isotopic distribution the highest peak in mass spectra of high-molecular weight compounds correlates better with molecular weight than with the mass of monoisotopic ion. Dell, A.; Morris, H. R.; Easton, R.; Haslam, S.; Panico, M.; Sutton-Smith, M.; Reason, A. J.; Khoo, K.-H. In Structural Analysis of Oligosaccharides: FAB-MS, ES-MS and MALDY-MS; Ernst, G. W. H. B., Sinay, P., Eds.; Wiley-VCH: New York, 2000; pp 865−914.